Measurement of the $t\bar{t}$ production cross section in $p\bar{p}$ collisions at $\sqrt{s} = 1.96$ TeV using events with large Missing E_T and jets

T. Aaltonen,[21] B. Álvarez González[v],[9] S. Amerio,[41] D. Amidei,[32] A. Anastassov,[36] A. Annovi,[17] J. Antos,[12] G. Apollinari,[15] J.A. Appel,[15] A. Apresyan,[46] T. Arisawa,[56] A. Artikov,[13] J. Asaadi,[51] W. Ashmanskas,[15] B. Auerbach,[59] A. Aurisano,[51] F. Azfar,[40] W. Badgett,[15] A. Barbaro-Galtieri,[26] V.E. Barnes,[46] B.A. Barnett,[23] P. Barria[cc],[44] P. Bartos,[12] M. Bauce[aa],[41] G. Bauer,[30] F. Bedeschi,[44] D. Beecher,[28] S. Behari,[23] G. Bellettini[bb],[44] J. Bellinger,[58] D. Benjamin,[14] A. Beretvas,[15] A. Bhatti,[48] M. Binkley,[15] D. Bisello[aa],[41] I. Bizjak[gg],[28] K.R. Bland,[5] B. Blumenfeld,[23] A. Bocci,[14] A. Bodek,[47] D. Bortoletto,[46] J. Boudreau,[45] A. Boveia,[11] B. Brau[a],[15] L. Brigliadori[z],[6] A. Brisuda,[12] C. Bromberg,[33] E. Brucken,[21] M. Bucciantonio[bb],[44] J. Budagov,[13] H.S. Budd,[47] S. Budd,[22] K. Burkett,[15] G. Busetto[aa],[41] P. Bussey,[19] A. Buzatu,[31] C. Calancha,[29] S. Camarda,[4] M. Campanelli,[33] M. Campbell,[32] F. Canelli[12],[15] A. Canepa,[43] B. Carls,[22] D. Carlsmith,[58] R. Carosi,[44] S. Carrillo[k],[16] S. Carron,[15] B. Casal,[9] M. Casarsa,[15] A. Castro[z],[6] P. Catastini,[15] D. Cauz,[52] V. Cavaliere[cc],[44] M. Cavalli-Sforza,[4] A. Cerri[f],[26] L. Cerrito[q],[28] Y.C. Chen,[1] M. Chertok,[7] G. Chiarelli,[44] G. Chlachidze,[15] F. Chlebana,[15] K. Cho,[25] D. Chokheli,[13] J.P. Chou,[20] W.H. Chung,[58] Y.S. Chung,[47] C.I. Ciobanu,[42] M.A. Ciocci[cc],[44] A. Clark,[18] G. Compostella[aa],[41] M.E. Convery,[15] J. Conway,[7] M.Corbo,[42] M. Cordelli,[17] C.A. Cox,[7] D.J. Cox,[7] F. Crescioli[bb],[44] C. Cuenca Almenar,[59] J. Cuevas[v],[9] R. Culbertson,[15] D. Dagenhart,[15] N. d'Ascenzo[t],[42] M. Datta,[15] P. de Barbaro,[47] S. De Cecco,[49] G. De Lorenzo,[4] M. Dell'Orso[bb],[44] C. Deluca,[4] L. Demortier,[48] J. Deng[c],[14] M. Deninno,[6] F. Devoto,[21] M. d'Errico[aa],[41] A. Di Canto[bb],[44] B. Di Ruzza,[44] J.R. Dittmann,[5] M. D'Onofrio,[27] S. Donati[bb],[44] P. Dong,[15] M. Dorigo,[52] T. Dorigo,[41] K. Ebina,[56] A. Elagin,[51] A. Eppig,[32] R. Erbacher,[7] D. Errede,[22] S. Errede,[22] N. Ershaidat[y],[42] R. Eusebi,[51] H.C. Fang,[26] S. Farrington,[40] M. Feindt,[24] J.P. Fernandez,[29] C. Ferrazza[dd],[44] R. Field,[16] G. Flanagan[r],[46] R. Forrest,[7] M.J. Frank,[5] M. Franklin,[20] J.C. Freeman,[15] Y. Funakoshi,[56] I. Furic,[16] M. Gallinaro,[48] J. Galyardt,[10] J.E. Garcia,[18] A.F. Garfinkel,[46] P. Garosi[cc],[44] H. Gerberich,[22] E. Gerchtein,[15] S. Giagu[ee],[49] V. Giakoumopoulou,[3] P. Giannetti,[44] K. Gibson,[45] C.M. Ginsburg,[15] N. Giokaris,[3] P. Giromini,[17] M. Giunta,[44] G. Giurgiu,[23] V. Glagolev,[13] D. Glenzinski,[15] M. Gold,[35] D. Goldin,[51] N. Goldschmidt,[16] A. Golossanov,[15] G. Gomez,[9] G. Gomez-Ceballos,[30] M. Goncharov,[30] O. González,[29] I. Gorelov,[35] A.T. Goshaw,[14] K. Goulianos,[48] A. Gresele,[41] S. Grinstein,[4] C. Grosso-Pilcher,[11] R.C. Group,[55] J. Guimaraes da Costa,[20] Z. Gunay-Unalan,[33] C. Haber,[26] S.R. Hahn,[15] E. Halkiadakis,[50] A. Hamaguchi,[39] J.Y. Han,[47] F. Happacher,[17] K. Hara,[53] D. Hare,[50] M. Hare,[54] R.F. Harr,[57] K. Hatakeyama,[5] C. Hays,[40] M. Heck,[24] J. Heinrich,[43] M. Herndon,[58] S. Hewamanage,[5] D. Hidas,[50] A. Hocker,[15] W. Hopkins[g],[15] D. Horn,[24] S. Hou,[1] R.E. Hughes,[37] M. Hurwitz,[11] U. Husemann,[59] N. Hussain,[31] M. Hussein,[33] J. Huston,[33] G. Introzzi,[44] M. Iori[ee],[49] A. Ivanov[o],[7] E. James,[15] D. Jang,[10] B. Jayatilaka,[14] E.J. Jeon,[25] M.K. Jha,[6] S. Jindariani,[15] W. Johnson,[7] M. Jones,[46] K.K. Joo,[25] S.Y. Jun,[10] T.R. Junk,[15] T. Kamon,[51] P.E. Karchin,[57] Y. Kato[n],[39] W. Ketchum,[11] J. Keung,[43] V. Khotilovich,[51] B. Kilminster,[15] D.H. Kim,[25] H.S. Kim,[25] H.W. Kim,[25] J.E. Kim,[25] M.J. Kim,[17] S.B. Kim,[25] S.H. Kim,[53] Y.K. Kim,[11] N. Kimura,[56] M. Kirby,[15] S. Klimenko,[16] K. Kondo,[56] D.J. Kong,[25] J. Konigsberg,[16] A.V. Kotwal,[14] M. Kreps,[24] J. Kroll,[43] D. Krop,[11] N. Krumnack[l],[5] M. Kruse,[14] V. Krutelyov[d],[51] T. Kuhr,[24] M. Kurata,[53] S. Kwang,[11] A.T. Laasanen,[46] S. Lami,[44] S. Lammel,[15] M. Lancaster,[28] R.L. Lander,[7] K. Lannon[u],[37] A. Lath,[50] G. Latino[cc],[44] I. Lazzizzera,[41] T. LeCompte,[2] E. Lee,[51] H.S. Lee,[11] J.S. Lee,[25] S.W. Lee[w],[51] S. Leo[bb],[44] S. Leone,[44] J.D. Lewis,[15] C.-J. Lin,[26] J. Linacre,[40] M. Lindgren,[15] E. Lipeles,[43] A. Lister,[18] D.O. Litvintsev,[15] C. Liu,[45] Q. Liu,[46] T. Liu,[15] S. Lockwitz,[59] N.S. Lockyer,[43] A. Loginov,[59] D. Lucchesi[aa],[41] J. Lueck,[24] P. Lujan,[26] P. Lukens,[15] G. Lungu,[48] J. Lys,[26] R. Lysak,[12] R. Madrak,[15] K. Maeshima,[15] K. Makhoul,[30] P. Maksimovic,[23] S. Malik,[48] G. Manca[b],[27] A. Manousakis-Katsikakis,[3] F. Margaroli,[46] C. Marino,[24] M. Martínez,[4] R. Martínez-Ballarín,[29] P. Mastrandrea,[49] M. Mathis,[23] M.E. Mattson,[57] P. Mazzanti,[6] K.S. McFarland,[47] P. McIntyre,[51] R. McNulty[i],[27] A. Mehta,[27] P. Mehtala,[21] A. Menzione,[44] C. Mesropian,[48] T. Miao,[15] D. Mietlicki,[32] A. Mitra,[1] H. Miyake,[53] S. Moed,[20] N. Moggi,[6] M.N. Mondragon[k],[15] C.S. Moon,[25] R. Moore,[15] M.J. Morello,[15] J. Morlock,[24] P. Movilla Fernandez,[15] A. Mukherjee,[15] Th. Muller,[24] P. Murat,[15] M. Mussini[z],[6] J. Nachtman[m],[15] Y. Nagai,[53] J. Naganoma,[56] I. Nakano,[38] A. Napier,[54] J. Nett,[51] C. Neu,[55] M.S. Neubauer,[22] J. Nielsen[e],[26] L. Nodulman,[2] O. Norniella,[22] E. Nurse,[28] L. Oakes,[40] S.H. Oh,[14] Y.D. Oh,[25]

I. Oksuzian,[55] T. Okusawa,[39] R. Orava,[21] L. Ortolan,[4] S. Pagan Griso[aa],[41] C. Pagliarone,[52] E. Palencia[f],[9]
V. Papadimitriou,[15] A.A. Paramonov,[2] J. Patrick,[15] G. Pauletta[ff],[52] M. Paulini,[10] C. Paus,[30] D.E. Pellett,[7]
A. Penzo,[52] T.J. Phillips,[14] G. Piacentino,[44] E. Pianori,[43] J. Pilot,[37] K. Pitts,[22] C. Plager,[8] L. Pondrom,[58]
K. Potamianos,[46] O. Poukhov,[13] F. Prokoshin[x],[13] A. Pronko,[15] F. Ptohos[h],[17] E. Pueschel,[10] G. Punzi[bb],[44]
J. Pursley,[58] A. Rahaman,[45] V. Ramakrishnan,[58] N. Ranjan,[46] I. Redondo,[29] P. Renton,[40] M. Rescigno,[49]
F. Rimondi[z],[6] L. Ristori[45],[15] A. Robson,[19] T. Rodrigo,[9] T. Rodriguez,[43] E. Rogers,[22] S. Rolli,[54] R. Roser,[15]
M. Rossi,[52] F. Rubbo,[15] F. Ruffini[cc],[44] A. Ruiz,[9] J. Russ,[10] V. Rusu,[15] A. Safonov,[51] W.K. Sakumoto,[47]
Y. Sakurai,[56] L. Santi[ff],[52] L. Sartori,[44] K. Sato,[53] V. Saveliev[t],[42] A. Savoy-Navarro,[42] P. Schlabach,[15]
A. Schmidt,[24] E.E. Schmidt,[15] M.P. Schmidt,[59] M. Schmitt,[36] T. Schwarz,[7] L. Scodellaro,[9] A. Scribano[cc],[44]
F. Scuri,[44] A. Sedov,[46] S. Seidel,[35] Y. Seiya,[39] A. Semenov,[13] F. Sforza[bb],[44] A. Sfyrla,[22] S.Z. Shalhout,[7]
T. Shears,[27] P.F. Shepard,[45] M. Shimojima[s],[53] S. Shiraishi,[11] M. Shochet,[11] I. Shreyber,[34] A. Simonenko,[13]
P. Sinervo,[31] A. Sissakian,[13] K. Sliwa,[54] J.R. Smith,[7] F.D. Snider,[15] A. Soha,[15] S. Somalwar,[50] V. Sorin,[4]
P. Squillacioti,[15] M. Stancari,[15] M. Stanitzki,[59] R. St. Denis,[19] B. Stelzer,[31] O. Stelzer-Chilton,[31] D. Stentz,[36]
J. Strologas,[35] G.L. Strycker,[32] Y. Sudo,[53] A. Sukhanov,[16] I. Suslov,[13] K. Takemasa,[53] Y. Takeuchi,[53] J. Tang,[11]
M. Tecchio,[32] P.K. Teng,[1] J. Thom[g],[15] J. Thome,[10] G.A. Thompson,[22] E. Thomson,[43] P. Ttito-Guzmán,[29]
S. Tkaczyk,[15] D. Toback,[51] S. Tokar,[12] K. Tollefson,[33] T. Tomura,[53] D. Tonelli,[15] S. Torre,[17] D. Torretta,[15]
P. Totaro[ff],[52] M. Trovato[dd],[44] Y. Tu,[43] F. Ukegawa,[53] S. Uozumi,[25] A. Varganov,[32] F. Vázquez[k],[16] G. Velev,[15]
C. Vellidis,[3] M. Vidal,[29] I. Vila,[9] R. Vilar,[9] M. Vogel,[35] G. Volpi[bb],[44] P. Wagner,[43] R.L. Wagner,[15] T. Wakisaka,[39]
R. Wallny,[8] S.M. Wang,[1] A. Warburton,[31] D. Waters,[28] M. Weinberger,[51] W.C. Wester III,[15] B. Whitehouse,[54]
D. Whiteson[c],[43] A.B. Wicklund,[2] E. Wicklund,[15] S. Wilbur,[11] F. Wick,[24] H.H. Williams,[43] J.S. Wilson,[37]
P. Wilson,[15] B.L. Winer,[37] P. Wittich[g],[15] S. Wolbers,[15] H. Wolfe,[37] T. Wright,[32] X. Wu,[18] Z. Wu,[5] K. Yamamoto,[39]
J. Yamaoka,[14] T. Yang,[15] U.K. Yang[p],[11] Y.C. Yang,[25] W.-M. Yao,[26] G.P. Yeh,[15] K. Yi[m],[15] J. Yoh,[15] K. Yorita,[56]
T. Yoshida[j],[39] G.B. Yu,[14] I. Yu,[25] S.S. Yu,[15] J.C. Yun,[15] A. Zanetti,[52] Y. Zeng,[14] and S. Zucchelli[z6]

(CDF Collaboration)

The CDF Collaboration
[1]*Institute of Physics, Academia Sinica, Taipei, Taiwan 11529, Republic of China*
[2]*Argonne National Laboratory, Argonne, Illinois 60439, USA*
[3]*University of Athens, 157 71 Athens, Greece*
[4]*Institut de Fisica d'Altes Energies, Universitat Autonoma de Barcelona, E-08193, Bellaterra (Barcelona), Spain*
[5]*Baylor University, Waco, Texas 76798, USA*
[6]*Istituto Nazionale di Fisica Nucleare Bologna, [z]University of Bologna, I-40127 Bologna, Italy*
[7]*University of California, Davis, Davis, California 95616, USA*
[8]*University of California, Los Angeles, Los Angeles, California 90024, USA*
[9]*Instituto de Fisica de Cantabria, CSIC-University of Cantabria, 39005 Santander, Spain*
[10]*Carnegie Mellon University, Pittsburgh, Pennsylvania 15213, USA*
[11]*Enrico Fermi Institute, University of Chicago, Chicago, Illinois 60637, USA*
[12]*Comenius University, 842 48 Bratislava, Slovakia; Institute of Experimental Physics, 040 01 Kosice, Slovakia*
[13]*Joint Institute for Nuclear Research, RU-141980 Dubna, Russia*
[14]*Duke University, Durham, North Carolina 27708, USA*
[15]*Fermi National Accelerator Laboratory, Batavia, Illinois 60510, USA*
[16]*University of Florida, Gainesville, Florida 32611, USA*
[17]*Laboratori Nazionali di Frascati, Istituto Nazionale di Fisica Nucleare, I-00044 Frascati, Italy*
[18]*University of Geneva, CH-1211 Geneva 4, Switzerland*
[19]*Glasgow University, Glasgow G12 8QQ, United Kingdom*
[20]*Harvard University, Cambridge, Massachusetts 02138, USA*
[21]*Division of High Energy Physics, Department of Physics,
University of Helsinki and Helsinki Institute of Physics, FIN-00014, Helsinki, Finland*
[22]*University of Illinois, Urbana, Illinois 61801, USA*
[23]*The Johns Hopkins University, Baltimore, Maryland 21218, USA*
[24]*Institut für Experimentelle Kernphysik, Karlsruhe Institute of Technology, D-76131 Karlsruhe, Germany*
[25]*Center for High Energy Physics: Kyungpook National University,
Daegu 702-701, Korea; Seoul National University, Seoul 151-742,
Korea; Sungkyunkwan University, Suwon 440-746,
Korea; Korea Institute of Science and Technology Information,
Daejeon 305-806, Korea; Chonnam National University, Gwangju 500-757,
Korea; Chonbuk National University, Jeonju 561-756, Korea*
[26]*Ernest Orlando Lawrence Berkeley National Laboratory, Berkeley, California 94720, USA*

^{27} *University of Liverpool, Liverpool L69 7ZE, United Kingdom*
^{28} *University College London, London WC1E 6BT, United Kingdom*
^{29} *Centro de Investigaciones Energeticas Medioambientales y Tecnologicas, E-28040 Madrid, Spain*
^{30} *Massachusetts Institute of Technology, Cambridge, Massachusetts 02139, USA*
^{31} *Institute of Particle Physics: McGill University, Montréal, Québec,*
Canada H3A 2T8; Simon Fraser University, Burnaby, British Columbia,
Canada V5A 1S6; University of Toronto, Toronto, Ontario,
Canada M5S 1A7; and TRIUMF, Vancouver, British Columbia, Canada V6T 2A3
^{32} *University of Michigan, Ann Arbor, Michigan 48109, USA*
^{33} *Michigan State University, East Lansing, Michigan 48824, USA*
^{34} *Institution for Theoretical and Experimental Physics, ITEP, Moscow 117259, Russia*
^{35} *University of New Mexico, Albuquerque, New Mexico 87131, USA*
^{36} *Northwestern University, Evanston, Illinois 60208, USA*
^{37} *The Ohio State University, Columbus, Ohio 43210, USA*
^{38} *Okayama University, Okayama 700-8530, Japan*
^{39} *Osaka City University, Osaka 588, Japan*
^{40} *University of Oxford, Oxford OX1 3RH, United Kingdom*
^{41} *Istituto Nazionale di Fisica Nucleare, Sezione di Padova-Trento, ^{aa} University of Padova, I-35131 Padova, Italy*
^{42} *LPNHE, Universite Pierre et Marie Curie/IN2P3-CNRS, UMR7585, Paris, F-75252 France*
^{43} *University of Pennsylvania, Philadelphia, Pennsylvania 19104, USA*
^{44} *Istituto Nazionale di Fisica Nucleare Pisa, ^{bb} University of Pisa,*
^{cc} *University of Siena and ^{dd} Scuola Normale Superiore, I-56127 Pisa, Italy*
^{45} *University of Pittsburgh, Pittsburgh, Pennsylvania 15260, USA*
^{46} *Purdue University, West Lafayette, Indiana 47907, USA*
^{47} *University of Rochester, Rochester, New York 14627, USA*
^{48} *The Rockefeller University, New York, New York 10065, USA*
^{49} *Istituto Nazionale di Fisica Nucleare, Sezione di Roma 1,*
^{ee} *Sapienza Università di Roma, I-00185 Roma, Italy*
^{50} *Rutgers University, Piscataway, New Jersey 08855, USA*
^{51} *Texas A&M University, College Station, Texas 77843, USA*
^{52} *Istituto Nazionale di Fisica Nucleare Trieste/Udine,*
I-34100 Trieste, ^{ff} University of Trieste/Udine, I-33100 Udine, Italy
^{53} *University of Tsukuba, Tsukuba, Ibaraki 305, Japan*
^{54} *Tufts University, Medford, Massachusetts 02155, USA*
^{55} *University of Virginia, Charlottesville, VA 22906, USA*
^{56} *Waseda University, Tokyo 169, Japan*
^{57} *Wayne State University, Detroit, Michigan 48201, USA*
^{58} *University of Wisconsin, Madison, Wisconsin 53706, USA*
^{59} *Yale University, New Haven, Connecticut 06520, USA*

In this paper we report a measurement of the $t\bar{t}$ production cross section in $p\bar{p}$ collisions at $\sqrt{s} = 1.96$ TeV using data corresponding to an integrated luminosity of 2.2 fb^{-1} collected with the CDF II detector at the Tevatron accelerator. We select events with significant missing transverse energy and high jet multiplicity. This measurement vetoes the presence of explicitly identified electrons and muons, thus enhancing the tau contribution of $t\bar{t}$ decays. Signal events are discriminated from the background using a neural network, and heavy flavor jets are identified by a secondary-vertex tagging algorithm. We measure a $t\bar{t}$ production cross section of 7.99 $\pm$ 0.55 (stat) $\pm$ 0.76 (syst) $\pm$ 0.46 (lumi) pb, assuming a top mass $m_{top} = 172.5$ GeV/c^2, in agreement with previous measurements and standard model predictions.

I. INTRODUCTION

In $p\bar{p}$ collisions at $\sqrt{s} = 1.96$ TeV at the Tevatron, top quarks are produced mainly in pairs through quark-antiquark annihilation and gluon-gluon fusion processes. In the standard model (SM), the calculated cross section for top pair production at the Tevatron center-of-mass energy is $7.46^{+0.66}_{-0.80}$ pb [1] for a top mass of 172.5 GeV/c^2. This value can be enhanced by new processes beyond the SM such as top pair production via new massive resonances [2], while the comparison of the top pair production cross section in different decay channels can be sen-

sitive to the presence of top decays via a charged Higgs boson [3]. Thus, a precise measurement of the top pair production cross section is an important test of the SM. Both CDF and D0 have performed many measurements of this quantity in different $t\bar{t}$ final states: the most recent published results, both measured in the decay channel with leptons and jets assuming $m_{top} = 172.5$ GeV/c^2, are 7.70 $\pm$ 0.52 pb for CDF [4] and 7.78 $^{+0.77}_{-0.64}$ pb for D0 [5].

As the Cabibbo-Kobayashi-Maskawa matrix element V_{tb} is close to unity [6, 7] and the top mass m_{top} is larger than the sum of the W boson and bottom quark (b)

masses, in the SM the $t \to Wb$ decay is dominant and has a branching ratio of about 100%. Since the W subsequently decays either to a quark-antiquark pair or to a lepton-neutrino pair, the resulting top pair production final states can be classified by the number of energetic charged leptons and the number of jets. When only one W decays leptonically, the $t\bar{t}$ event is characterized by the presence of a charged lepton, missing energy due to the undetected neutrino, and four high energy jets, two of which originate from b quarks. In this *lepton plus jets* channel, one selects events with an energetic electron or muon. For this paper we focus on an inclusive high-momentum neutrino signature of large missing energy accompanied by jets. By not explicitly requiring leptons, our measurement is sensitive to all W leptonic decay modes including τ decays of W's: about 40% of the signal sample obtained after the kinematic selection contains events with a τ lepton in the final state. To ensure our measurement is statistically independent from other CDF results [8], we veto events with high-momentum electrons or muons as well as multijet events with no leptons (*all-hadronic $t\bar{t}$ decays*). This choice is expected to improve the final CDF combined cross section value: the previous 311 pb^{-1} result [9] carried a weight of about 17% in the combination.

One of the major challenges of this measurement is the large background from QCD multijet processes and electroweak production of W bosons associated with b and c jets (heavy flavor jets), which dominates the signal by two orders of magnitude before any selection. In order to improve the signal to background ratio (S/B), a neural network is trained to identify the kinematic and topological characteristics of SM $t\bar{t}$ events, and is applied to data to select a signal-rich sample. Top quarks are then identified by their distinctive decay into b quarks. Jets originating from b quarks (b jets) are selected ("tagged") by their displaced vertex as defined by the SECVTX algorithm [10]. After evaluating the average number of b-tagged jets for $t\bar{t}$ events using a Monte Carlo (MC) simulation, the number of signal events in the sample and the corresponding cross section are measured by counting the number of b tags in the sample selected by the neural network. The number of background b tags is estimated using per-jet parametrized probabilities of b-jet identification, measured directly from data, rather than relying on theoretical prediction of cross sections and MC simulations. The results reported here are based on data taken between March 2002 and August 2007, corresponding to an integrated luminosity of 2.2 fb^{-1}, recorded by the CDF experiment at Fermilab.

The organization of the paper is the following: Sec. II contains a brief description of the CDF II detector and of the trigger requirements used for this analysis. The preliminary clean-up cuts applied to data are described in Sec. III, followed by the discussion of the data-driven background parametrization in Sec. IV. The kinematic variables characterizing the missing energy plus jets final state and the neural network based sample selection are described in Sec. V and in Sec. VI respectively. We conclude the description of this measurement with a summary of the different sources of systematic uncertainties in Sec. VII, while the cross section measurement is presented in Sec. VIII.

II. THE CDF DETECTOR AND TRIGGER SYSTEM

CDF II is a general–purpose, azimuthally and forward-backward symmetric detector located at the Tevatron $p\bar{p}$ collider at Fermilab. It consists of a charged-particle tracking system immersed in a 1.4 T magnetic field. The solenoid is surrounded by calorimeters and muon detectors [11]. The CDF II coordinate system uses θ and ϕ as the polar and azimuthal angles respectively, defined with respect to the proton beam axis direction, z. The x-axis points towards the center of the accelerator while the y axis upwards from the beam. The pseudorapidity η is defined as $\eta \equiv -\ln[\tan(\theta/2)]$. The transverse momentum of a particle is $p_T = p\sin\theta$ and its transverse energy $E_T = E\sin\theta$. The missing transverse energy $\not{E}_T$ measures the transverse energy of the neutrinos via the imbalance of the energy detected in the calorimeters; it is defined by $\not{E}_T = |\vec{\not{E}}_T|$ where $\vec{\not{E}}_T = -\sum_i E_T^i \hat{n}_i$, the index i runs over the calorimeter tower number and $\hat{n}_i$ is a unit vector perpendicular to the beam axis and pointing at the i-th calorimeter tower. The tracking system is composed of 8 layers of silicon microstrip detectors, extending from 1.6 cm to 28 cm and covering up to $|\eta| < 2.0$, surrounded by a 3.1 m long open cell drift chamber, providing $|\eta|$ coverage up to 1.0. Using information from the silicon detectors, the primary interaction vertex is reconstructed with a precision of ~ 15 μm in the plane transverse to the beam [12]. The energy of the particles traversing the detector is measured by electromagnetic and hadronic calorimeters segmented into projective towers covering up to $|\eta| < 3.6$. In the central region ($|\eta| < 1.1$) the calorimetric towers are 15° wide in ϕ and 0.1 in η; in the forward region ($1.1 < |\eta| < 3.6$) the towers are 7.5° wide in azimuthal angle for $|\eta| < 2.1$ and 15° for $|\eta| > 2.1$. The electromagnetic section is made of lead-scintillator plates, while the hadronic section uses iron-scintillator ones. The transverse profile of electromagnetic showers is measured by proportional chambers and scintillating strip detectors. Muons are detected up to $|\eta| < 0.6$ by drift chambers located outside the hadronic calorimeters, behind a 60 cm iron shield. Additional drift chambers and scintillator detectors provide muon detection up to $|\eta| < 1.5$.

The CDF II trigger system [13] has a three level architecture designed to reduce the data rate from 2.53 MHz, the bunch crossing frequency, to approximately 120 Hz to be written on tape. The data used in this measurement are collected with a purely calorimetric trigger, described in Sec. II A. At Level-1 (L1) calorimetric towers are merged in pairs along η to define *trigger towers*: the

L1 can take a decision on the total energy contribution of individual trigger towers or on the total transverse energy and the missing transverse energy of the event. At Level-2 (L2) trigger towers are merged into clusters by a simple clustering algorithm [14], while at Level-3 (L3) jets of particles are reconstructed by a fixed cone-based algorithm [15], the radius of the cone in the $\eta - \phi$ plane ($\Delta R = \sqrt{\Delta\eta^2 + \Delta\phi^2}$) being 0.4, 0.7 or 1 depending on the specific trigger.

A. The Multijet trigger

The data used in this analysis are collected by a multi-jet trigger. This trigger requires at L1 the presence of at least one central trigger tower with $E_T \geq 10$ GeV, and at L2 at least four calorimetric clusters with $E_T \geq 15$ GeV each and a total transverse energy greater than 175 GeV. The latter threshold was 125 GeV before February 2005 and was increased to reduce the trigger rate at higher instantaneous luminosity. Finally, at L3, at least four jets with $E_T \geq 10$ GeV ($\Delta R = 0.4$) are required. This trigger was specifically designed to collect all-hadronic $t\bar{t}$ events, where the final state nominally consists of six jets, but has a large acceptance also on final states characterized by $\not{E}_T$ and high jet multiplicity. Moreover the collected sample is uncorrelated with those used for top cross section measurements in the lepton plus jets final state, which are selected by requiring the presence of a high momentum lepton. The choice of this trigger is also driven by the analysis strategy: the top cross section measurement is performed by counting the number of b-tagged jets from top decay in the final sample and the multijet trigger provides a sample that is unbiased with respect to the b-tagging algorithm, as it does not apply any requirement on tracks.

III. PRELIMINARY REQUIREMENTS

Events satisfying the trigger requirements are used in the analysis only if they were collected with fully operational tracking detectors, calorimeters and muon systems, and if their primary vertex is located within $\pm$ 60 cm along z from the center of CDF II detector. Jets and $\not{E}_T$ are corrected [16] for multiple $p\bar{p}$ interactions in the event, non uniformities in the calorimeter response along η, and any non-linearity and energy loss in the uninstrumented regions of the calorimeters. The $\not{E}_T$ is also corrected for the presence of high-p_T muons. We consider jets with $\Delta R = 0.4$, corrected transverse energy $E_T \geq 15$ GeV and $|\eta| \leq 2.0$; the total transverse energy of the event $\sum E_T$ is defined as the sum of all jets E_T.

Events are required to have at least three jets and no central high-p_T ($p_T > 20$ GeV/c) reconstructed electrons or muons to avoid overlaps with other top cross section measurements in lepton and jets final states [17]. In the same way, overlaps with top all-hadronic analyses are

avoided by rejecting events with low $\not{E}_T$ significance $\not{E}_T^{sig}$, defined as $\not{E}_T^{sig} = \not{E}_T / \sqrt{\sum E_T}$, as the resolution on the $\not{E}_T$ is observed to degrade as a function of the total transverse energy of the event. The $\not{E}_T^{sig}$ is typically low when $\not{E}_T$ arises from mismeasurements, so events are required to have $\not{E}_T^{sig} \geq 3$ GeV$^{1/2}$.

Throughout the paper, the impact of analysis requirements on signal is evaluated using inclusive $t\bar{t}$ samples generated with PYTHIA version v6.216 [18] and processed through CDF II detector and full trigger simulation [19], assuming a top mass $m_{top} = 172.5$ GeV/c^2 (the most recent CDF and D0 combined result on top mass is $m_{top} = 173.3 \pm 1.1$ GeV/c^2 [20]). After the preliminary cuts, there are 94 217 events remaining in the sample with at least four jets, with an expected signal to background ratio S/B of 1.4% and 44 310 events in the sample with exactly three jets, with an expected S/B lower than 0.1%. The latter sample, with a very low $t\bar{t}$ signal contamination, will be used to derive the background parametrization in Sec. IV.

IV. BACKGROUND PARAMETRIZATION

In this analysis, top quarks are identified by their decays into b quarks. However, many processes other than the decay of the top quark can give rise to b jets, therefore a procedure to estimate the number of b tags yielded by background processes is needed.

The background-prediction method used in this analysis rests on the assumption that the probabilities of tagging a b jet in $t\bar{t}$ signal and background processes are different: the differences are due to the distinctive properties of b jets produced by the top quark decays, compared to b jets arising from QCD and W boson plus heavy flavor production processes. In this hypothesis, parametrizing the b-tag rates as a function of jet variables in events depleted of signal allows one to predict the number of b-tagged jets from background processes in any given sample. The parametrization is derived from a sample of pure background: the data sample after the prerequisites requirement with exactly three jets, where the $t\bar{t}$ signal contamination is lower than 0.1%. In this sample the per-jet b-tagging probability is found to depend mainly on jet E_T, the number of good quality tracks contained in the jet cone N_{trk}, and the $\not{E}_T$ projection along the jet direction $\not{E}_T^{prj}$, defined as $\not{E}_T^{prj} = \not{E}_T \cos \Delta\phi(\not{E}_T, jet)$. These variables are chosen for the parametrization and their corresponding tag rate dependence is shown in Fig. 1. We expect the tagging probability to depend on jet E_T and N_{trk} due to the implementation details of the b-tagging algorithm [10]. In more detail, the b-tagging probability decreases at high jet E_T due to the declining yield of tracks passing the quality cuts required by the b-tagging algorithm; it increases if a greater number of good quality tracks is associated to the jet cone. The $\not{E}_T$ projection along the jet direction is correlated with the heavy flavor component of the sample and the geomet-

ric properties of the event. Neutrinos from the b-quark semi-leptonic decays force $\not{E}_T$ to be aligned with the jet direction, while neutrinos from W boson decays are more likely to be away from jets. For this reason the b-tag rate is enhanced at high positive values of $\not{E}_T^{prj}$.

A 3-dimensional b-tagging matrix $\mathcal{P}$ is defined using the per-jet b-tagging probabilities, and its binning is defined to avoid any entries with empty denominators. The matrix assigns the probability that a jet is b-tagged given its E_T, N_{trk} and $\not{E}_T^{prj}$.

The total number of expected background b tags N_{exp} in a given data sample can be calculated by summing the b-tagging probabilities over all jets in the selected events:

$$N_{exp} = \sum_{i=1}^{N_{events}} \sum_{k=1}^{N_{jets,i}} \mathcal{P}_i(E_T^k, N_{trk}^k, \not{E}_T^{prj,k}) \qquad (1)$$

where the index k runs over the number of jets N_{jets} in the i-th event and the index i runs over all the N_{events} events in the sample. Due to the method we used, N_{exp} is obtained under the same assumption that allowed the parametrization of the tagging rate, i.e. a negligible $t\bar{t}$ signal contamination. For jet multiplicities greater than three, N_{exp} will overestimate the number of b tags from background events, N_{bkg}, due to the presence of $t\bar{t}$ events in the sample. If N_{obs} is the number of b tags observed in the data sample and we assume that the difference between N_{obs} and N_{bkg} is due to the presence of $t\bar{t}$ signal, the number of top events in the sample n_{top} can be evaluated as $n_{top} = (N_{obs} - N_{bkg})/\epsilon_{tag}^{ave}$, where ϵ_{tag}^{ave} is the average number of b tags per top event, defined as the ratio between the number of b-tagged jets and the number of $t\bar{t}$ events and calculated from MC simulation. If n_{evt} is the number of events in the sample, we can estimate the number of b tags due to the background N_{bkg}, by rescaling the value N_{exp} predicted by the b-tagging matrix as follows: $N_{bkg} = N_{exp}(n_{evt} - n_{top})/n_{evt}$. Putting the expressions for N_{bkg} and n_{top} together, we can evaluate N_{bkg} as the limit of the following iterative formula:

$$N_{bkg} = \lim_{i \to \infty} N_{exp,i} \qquad (2)$$

with

$$N_{exp,i} = N_{exp,0} \frac{n_{evt} - n_{top}}{n_{evt}}$$
$$= N_{exp,0} \frac{n_{evt} - (N_{obs} - N_{exp,i-1})/\epsilon_{tag}^{ave}}{n_{evt}} \qquad (3)$$

where $N_{exp,0} = N_{exp}$ is the number - fixed during the iteration - of expected tags coming from the tag rate parametrization before any correction. In our calculations the iterative procedure stops when $\frac{|N_{exp,i} - N_{exp,i-1}|}{N_{exp,i}} \leq 1\%$. This correction procedure is used in all samples with more than three jets to remove the $t\bar{t}$ contribution from the background estimation. This method does not require knowledge of the top production cross section, once we assume that the dependence

of ϵ_{tag}^{ave} from the top quark mass is negligible.

To ensure the correct behavior of the b-tagging parametrization, an important check consists in calculating the predicted number of b tags in data samples with jet multiplicities higher than three, and compare it with the actual observed number of b-tagged jets. The result of this check is shown in Fig. 2. Taking into account the expected contribution to the number of observed b tags due to the presence of $t\bar{t}$ events in the sample ($m_{top} = 172.5$ GeV/c^2), the agreement between the amount of observed and predicted b tags is good in all the jet multiplicity bins, being exactly the same by definition for 3-jet events, on which the parametrization is calculated.

V. SIGNAL AND BACKGROUND CHARACTERIZATION

In the data sample under investigation, $t\bar{t}$ pairs are overwhelmed by multijet QCD and W + jets events. The main feature of the $t\bar{t}$ decay channel analyzed here is a considerable amount of $\not{E}_T$, the only observable signature of the presence of neutrinos from W leptonic decays. However, missing transverse energy can be also produced by jet energy mismeasurements, by semi-leptonic decays of b quarks in QCD events and by the leptonic decay of the W in W + jets events. To discriminate against the possible sources of missing transverse energy on a geometric basis we use the quantity $\Delta\phi_{min} = \min \Delta\phi(\not{E}_T, jet)$, defined as the minimum angular difference between the $\not{E}_T$ and each jet in the event. This quantity is expected to be large in $W \to l\nu$ decays and in $t\bar{t} \to \not{E}_T$ + jets events. On the other hand, for QCD background events where the main source of $\not{E}_T$ is due to jet energy mismeasurement, the $\not{E}_T$ is expected to be aligned with the jet direction and the value of $\Delta\phi_{min}$ close to zero.

Other kinematic variables related to the topology of the event characterize the $t\bar{t}$ production with respect to background processes. Let $Q_{j(j=1,3)}$ be the eigenvalues of the normalized momentum tensor $M_{ab} = \frac{\sum_j P_{ja}P_{jb}}{\sum_j P_j^2}$ [21], where a, b run over the three space coordinates, and P_j is the momentum of the jet j. The sphericity S is defined as $S = \frac{3}{2}(1 - Q_3)$. S is zero in the limiting case of a pair of back-to-back jets, while approaches one for events with a perfectly isotropic jet momenta distribution. The aplanarity A is defined as $A = \frac{3}{2}Q_1$ and lies in the range $[0, \frac{1}{2}]$. Extremal values of A are reached in the case of two opposite jets and in the case of evenly distributed jets, respectively. Jets emerging from a $t\bar{t}$ pair are expected to be uniformly distributed and, as a consequence, they will hardly lie on the same plane: thus we expect high aplanarity and sphericity values for $t\bar{t}$ events. In addition to kinematic variables describing the topology of the event, distributions of energy-related variables can be useful to discriminate $t\bar{t}$ events over their background. The cen-
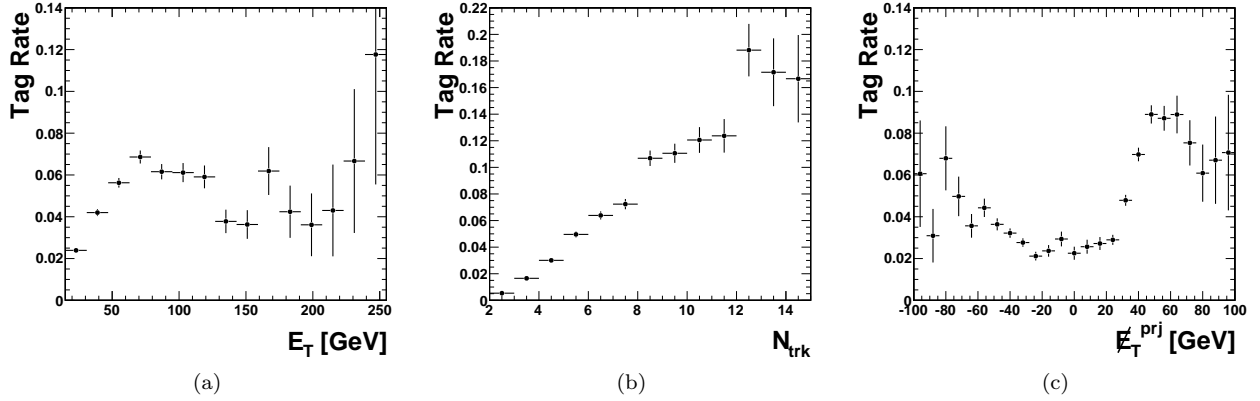
FIG. 1. b tagging rates as a function of jet E_T (a), N_{trk} (b) and $\not{E}_T^{\,prj}$ (c) for the data sample with exactly three jets in the event.
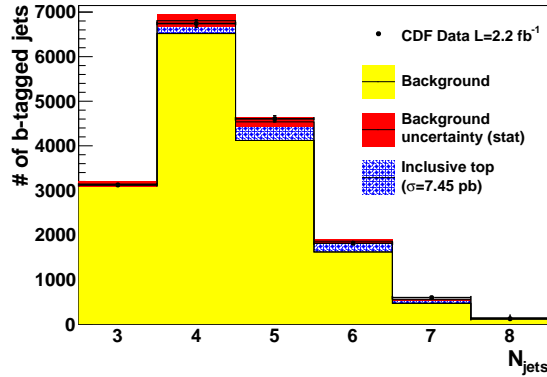

FIG. 2. Tagging matrix check on data after preliminary requirements and before any additional kinematic selection. Observed and predicted number of b-tagged jets as a function of the jet multiplicity are shown in the figure, statistical errors only. The expected contribution coming from $t\bar{t}$ events based on the theoretical cross section of $\sigma_{t\bar{t}} = 7.45$ pb is also shown. Background error bands are centered on the inclusive top plus background prediction.

trality C is defined as $C = \frac{\sum E_T}{\sqrt{\hat{s}}}$, where $\sqrt{\hat{s}}$ is the center of mass energy in the hard scattering reference frame. In the case of $t\bar{t}$ pairs decaying hadronically, jets are emitted preferably in the transverse plane ($r - \phi$ plane), so we expect to have a greater amount of energy emitted in this plane giving values of C closer to 1 with respect to background events. The variable $\sum_3 E_T$ is defined as the sum of all jets E_T in the event except the two leading ones. In QCD events, the two most energetic jets are produced by $q\bar{q}$ processes, while the least energetic ones come from gluon *bremsstrahlung*; on the contrary, in $t\bar{t}$ events up to six jets can be produced by hard processes, and as a consequence $\sum_3 E_T$ can help discriminating signal and background. All these variables will be used in the following section to train a neural network to discriminate $t\bar{t}$ signal from background.

VI. NEURAL NETWORK BASED EVENT SELECTION

In order to enhance the signal to background ratio in the data sample, we use a neural network (NN), trained to discriminate $t\bar{t} \to \not{E}_T +$ jets signal events from background. The NN is built using the neural network implementation in ROOT [22].

We apply an additional kinematic requirement on data with at least four jets, removing events with low angle between jets and $\not{E}_T$ with the cut $\Delta\phi_{min}(\not{E}_T, jets) > 0.4$. In the data these events come mostly from mismeasured jets and are difficult to simulate in MC. They are removed from the NN training to prevent it from converging on artificial differences between MC and data rather than real physics effects. After this requirement, we are left with 20 043 events in the sample with at least four jets, with an expected S/B of 3.5%: since this sample has low $t\bar{t}$ signal contamination and no overlap with data used to determine the background parametrization, it will be used as background training sample. As signal training sample we use the same amount of events passing the same event selection of data, taken randomly from the $t\bar{t}$ simulation. We use as inputs for the network the following kinematic variables, normalized with respect to their maximum values: the transverse energy of the leading jet E_T^1, $\Delta\phi_{min}(\not{E}_T, jet)$, $\not{E}_T^{\,sig}$, $\sum E_T$, $\sum_3 E_T$, the centrality C, and the topology-related variables sphericity S and aplanarity A. The distributions of the input variables used in the NN for both the signal and background training samples are shown in Fig. 3.

After the training, the b-tagged data are processed by the NN: Fig. 4 shows the number of observed b-tagged jets versus the NN output NN_{out}, along with the corresponding background prediction from the tag rate parametrization and expected contribution from $t\bar{t}$ signal ($m_{top} = 172.5$ GeV/c^2), for events with at least four jets and with exactly three, four and five jets. The good agreement between data and the sum of expected back-
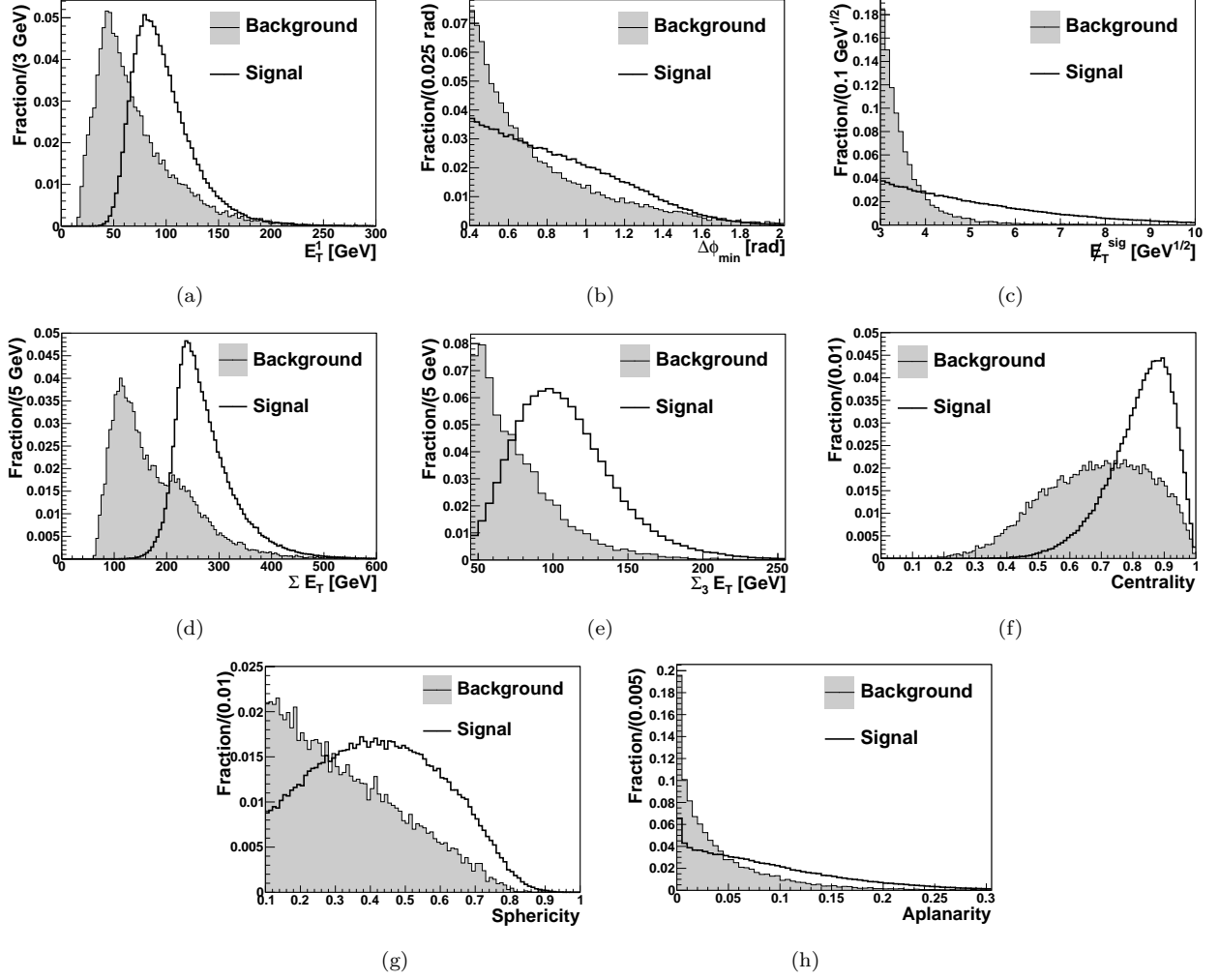
FIG. 3. Distribution of neural network input variables for multijet data (background) and $t\bar{t}$ MC (signal) samples: the transverse energy of the leading jet E_T^1 (a), $\Delta\phi_{min}(\not{E}_T, jet)$ (b), $\not{E}_T^{sig}$ (c), $\sum E_T$ (d), $\sum_3 E_T$ (e), the centrality C (f), and the topology-related variables sphericity S (g) and aplanarity A (h).

ground and $t\bar{t}$ induced b tags in the high NN output region is both a confirmation of the effectiveness of the method we use to estimate the background and a demonstration of proper NN training and performance.

In order to select a signal-rich sample to perform the cross section measurement, we choose to cut on the NN output value NN_{out}. The cut is chosen with the aim of minimizing the statistical uncertainty on the cross section measurement, maximizing S/B where S is the expected number of b tags from the signal and B is the predicted number of background b tags. The former quantity is evaluated from an inclusive $t\bar{t}$ MC sample, while the latter is derived using the b-tagging matrix parametrization on data. The result of this optimization procedure is a cut on $NN_{out} \geq 0.8$, which gives the lowest expected statistical uncertainty on the cross section ($\sim 8\%$) and an expected $S/B \sim 4$. The expected signal sample composition after this cut is shown in Table I.

VII. SYSTEMATIC UNCERTAINTIES

The top quark pair production cross section is measured as:

$$\sigma(p\bar{p} \rightarrow t\bar{t}) \times BR(t\bar{t} \rightarrow \not{E}_T + jets) = \frac{N_{obs} - N_{exp}}{\epsilon_{kin} \cdot \epsilon_{tag}^{ave} \cdot L} \quad (4)$$

where N_{obs} and N_{exp} are the number of observed and predicted tagged jets from background in the selected sample, respectively; ϵ_{kin} is the kinematic efficiency of trigger, preliminary requirements and neural network selection determined using inclusive MC $t\bar{t}$ events; ϵ_{tag}^{ave}, defined as the ratio of the number of b-tagged jets to the number of events in the inclusive $t\bar{t}$ Monte Carlo sample, gives the average number of b tags per $t\bar{t}$ event. Finally, L is the integrated luminosity of the dataset used. All quantities in the denominator of Eq. 4, as well as the
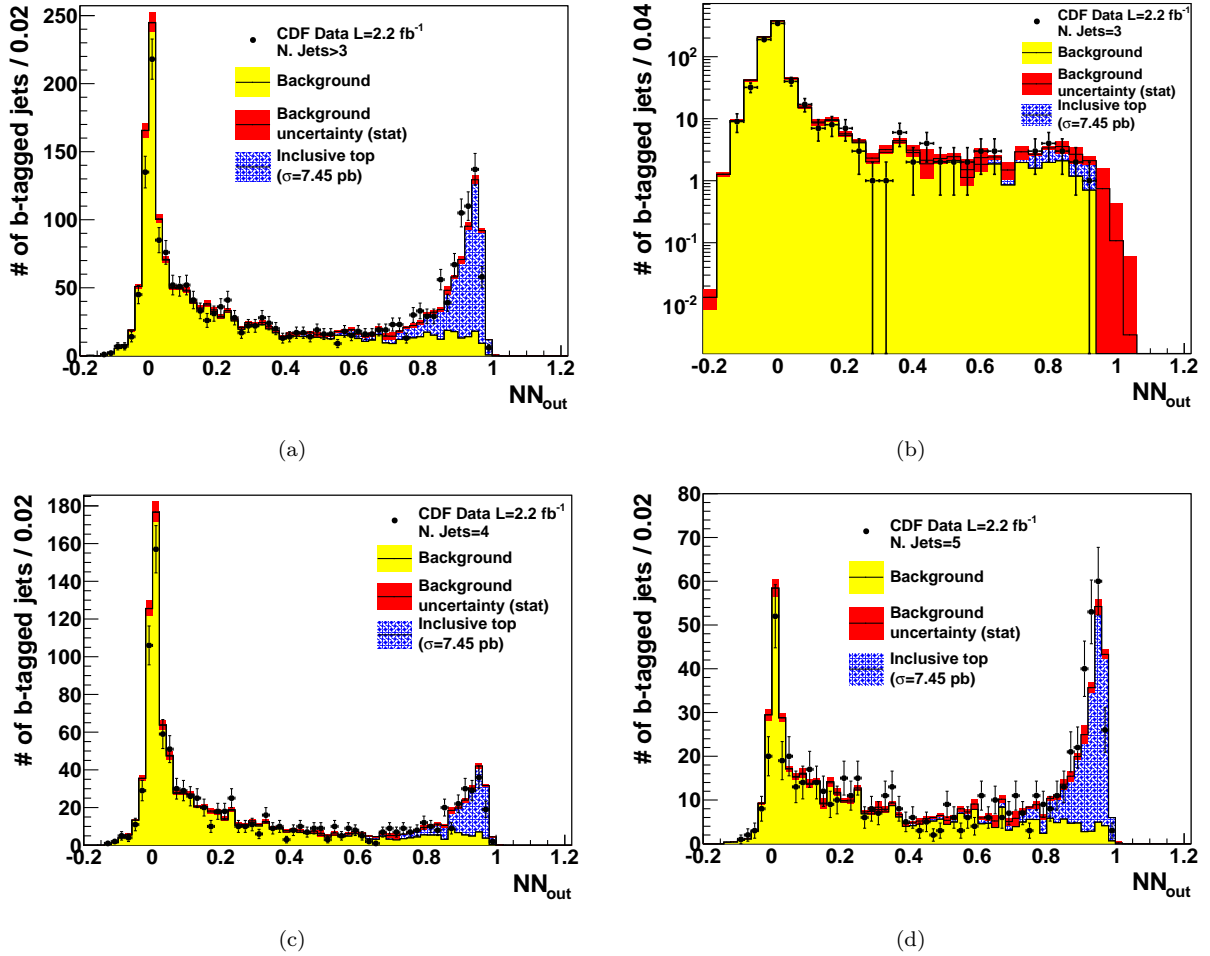
FIG. 4. Observed and matrix-predicted number of b-tagged jets versus neural network output in the multijet data for all events with at least four jets (a) and for events with exactly three (b), four (c) and five (d) jets, along with the expected contribution due to $t\bar{t}$ signal events. Background error bands are centered on the inclusive top plus background prediction.

TABLE I. Expected signal sample composition after the $NN_{out} > 0.8$ cut.

Number of jets	3	4	5	6	7	8	9	Total
all-hadronic (%)	0.1	0.5	1.7	4.9	7.8	10.2	9.9	2.3
e +jets (%)	26.7	25.2	35.5	36.2	35.1	33.6	33.8	32.1
μ +jets (%)	32.2	32.5	19.1	15.8	14.5	16.1	12.9	22.7
dileptonic (%)	6.5	2.3	1.1	0.7	0.5	0.6	0.00	1.4
hadronic τ +jets (%)	15.8	21.9	30.5	31.5	31.8	29.9	34.4	27.7
leptonic τ +jets (%)	11.7	13.2	9.9	9.1	8.9	8.1	8.4	10.8
$\tau\tau$ (%)	1.1	1.1	0.6	0.5	0.4	0.4	0.3	0.8
$e/\mu + \tau$ (%)	6.0	3.4	1.6	1.3	0.9	1.1	0.3	2.2

number of expected tags, are subject to different sources of systematic uncertainties.

The kinematic efficiency ϵ_{kin} is evaluated on inclusive $t\bar{t}$ samples generated with PYTHIA and its uncertainty arises from the particular choice of the MC generator, the set of parton density functions used in the generator, as well as the modeling of color reconnection effects and

of the initial and final state radiation.

The MC generators differ in their hadronization schemes and in their description of the underlying event and multiple interactions: in order to evaluate the generator dependence of the kinematic efficiency, we compare the value of ϵ_{kin} obtained using PYTHIA with the value obtained on a sample of events generated with HERWIG

v6.510 [23], and take the relative difference as the systematic uncertainty.

The choice of proton parton distribution function (PDF) affects the kinematics of $t\bar{t}$ events, and thus the acceptance for signal events. We estimate this uncertainty comparing the ϵ_{kin} value derived from MC samples based on the default PDF CTEQ5L [24] with the one obtained using samples based on MRST72 and MRST75 [25], which differ by the value of the strong coupling constant α_s used to compute the PDF; we also consider the difference in the value of ϵ_{kin} obtained with the leading order (LO) and next to leading order (NLO) calculations of PDFs, evaluated using default CTEQ5L (LO) and CTEQ6M (NLO) PDFs, and derive the corresponding uncertainty. We add these two contributions in quadrature to obtain the systematic uncertainty due to our choice of PDF.

Uncertainties arising from the modeling of color reconnections effects are estimated by evaluating the shift in the kinematic efficiency using two samples of events generated by PYTHIA, corresponding to different models of color reconnection [26].

Additional jets coming from initial and final state radiation (ISR and FSR), might change the sample composition and affect the efficiency of the kinematic selection. The systematic uncertainty related to these effects is evaluated by calculating the shift in ϵ_{kin} using inclusive $t\bar{t}$ samples with different amounts of initial and final state radiation.

The systematic uncertainty due to the calorimeter response is accounted for by varying the corrected jet energies within $\pm 1\sigma$ of their corresponding systematic uncertainty, and recalculating ϵ_{kin} after these variations.

Finally, ϵ_{kin} is also affected by the simulation of the trigger requirements on MC events and a trigger acceptance uncertainty is determined by comparing trigger turn-on curves between MC and data events.

The average number of b tags per $t\bar{t}$ event is affected by the uncertainty on the scale factor used to account for the different efficiency of the b-tagging algorithm in data and in MC. The systematic uncertainty on ϵ_{tag}^{ave} is obtained varying the scale factor within the $\pm 1\sigma$ range from its central value and determining, on the MC sample, the difference in terms of average number of b tags per event with respect to the standard ϵ_{tag}^{ave} value.

The uncertainty on the number N_{exp} of matrix-predicted b-tagged jets is calculated by comparing the number of b tags yielded by the tagging matrix to the actual number of observed SECVTX tags in a control sample depleted of signal contamination (events with NN output lower than 0.6). The relative difference between the expected and observed number of tagged jets is taken as an estimate of the uncertainty of our background prediction.

The luminosity measurement is affected by two sources of uncertainty: the acceptance of the luminosity monitor and the total inelastic $p\bar{p}$ cross section (60.7 ± 2.4 mb). The uncertainties on these quantities are 4.2% and 4.0% respectively, giving a total uncertainty of 5.8% on

TABLE II. Summary of relative systematic uncertainties on the signal efficiency, and other uncertainties related to the cross section evaluation.

Source	Uncertainty
ϵ_{kin} systematics	
Generator dependence	3.9 %
PDFs	1.2 %
ISR/FSR	2.7 %
Color Reconnection	4.3 %
Jet Energy Scale	4.2 %
Trigger simulation	3.0 %
Other systematics	
ϵ_{tag}^{ave} (b-tag scale factor)	3.9 %
Background parametrization	2.5 %
Luminosity measurement	5.8 %

TABLE III. Input values for the cross section measurement. ϵ_{tag}^{ave} is the average number of b tags per top event.

Variable	Symbol	Value
Integrated Luminosity (pb^{-1})	L	2207.5 ± 128
Observed b tags	N_{obs}	636
Background b tags	N_{bkg}	131 ± 9.6
Kinematic efficiency (%)	ϵ_{kin}	3.53 ± 0.29
Average b tagging efficiency (%)	ϵ_{tag}^{ave}	81.1 ± 3.2

the integrated luminosity calculated for any given CDF dataset.

The summary of all sources of systematic uncertainties to the cross section evaluation is listed in Table II.

VIII. CROSS SECTION MEASUREMENT

After the neural network selection we are left with 1420 events with at least four jets of which 636 are b-tagged. Inserting in Eq. 4 the input parameters quoted in Table III, the measured cross section value is

$$\sigma_{t\bar{t}} = 7.99 \ \pm 0.55 \ \text{(stat)} \ \pm 0.76 \ \text{(syst)} \ \pm 0.46 \ \text{(lumi) pb}$$
$$= 7.99 \ \pm 1.05 \ \text{pb}$$

Observed and expected b tags after selection for different jet multiplicities are shown in Fig. 5, along with the expected contribution of inclusive $t\bar{t}$ signal, normalized to the measured cross section.

IX. CONCLUSIONS

We presented a measurement of the $t\bar{t}$ production cross section in a final state with large missing transverse en-
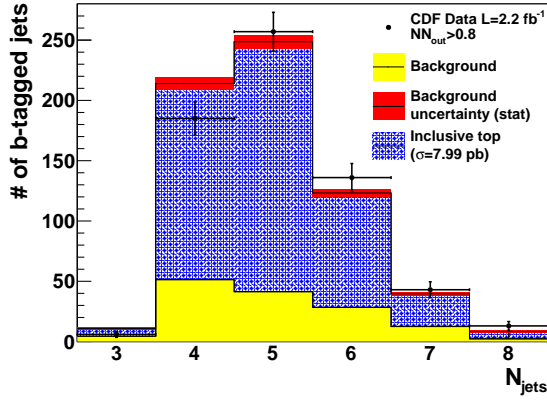
FIG. 5. Observed and matrix-predicted number of b-tagged jets by jet multiplicity in the multijet data after cut on neural network output NN_{out} greater than 0.8, along with the expected contribution of inclusive $t\bar{t}$ signal normalized to the measured cross section. Background error bands are centered on the inclusive top plus background prediction.

ergy and multiple jets. We explicitly vetoed well identified high-p_T electrons or muons from W boson decay, and rejected events with low missing transverse energy, to avoid overlaps with other cross section measurements performed by the CDF Collaboration. Using an optimized neural network based kinematic selection and a b jet identification technique on a sample of data corresponding to an integrated luminosity of 2.2 fb^{-1}, we obtain a production cross section value of 7.99 ± 1.05 pb, in good agreement with the reference theoretical value of

$7.46^{+0.66}_{-0.80}$ pb [1] and with other next to next to leading order calculations [27] for a top mass of 172.5 GeV/c^2. The agreement with the most recent experimental determinations is also good. Given the limited error of the result, this independent cross section measurement will have a significant impact on a future CDF combined value. The same $\rlap{/}{E}_T$ + jets sample can be used to measure the top quark mass: the overall uncertainty on the combined top mass value will benefit from a result statistically uncorrelated with those of other methods.

ACKNOWLEDGMENTS

[1] U. Lagenfeld, S. Moch, and P. Uwer, Phys. Rev. D **80**, 054009 (2009).

[2] C. T. Hill, Phys. Lett. B **266**, 419 (1991); T. Aaltonen *et al.* (CDF Collaboration), Phys. Rev. Lett. **100**, 231801 (2008).

[3] R. Dermíšek and J. F. Gunion, Phys. Rev. D **79**, 055014 (2009).

[4] T. Aaltonen *et al.* (CDF Collaboration), Phys. Rev. Lett. **105**, 012001 (2010).

[5] V. M. Abazov *et al.* (D0 Collaboration), arXiv:1101.0124v1 [hep-ex] (2010).

[6] V. M. Abazov *et al.* (D0 Collaboration), Phys. Rev. Lett. **103**, 092001 (2009).

[7] T. Aaltonen *et al.* (CDF Collaboration), Phys. Rev. Lett. **103**, 092002 (2009); T. Aaltonen *et al.* (CDF Collaboration), Phys. Rev. D **81**, 072003 (2010).

[8] T. Aaltonen *et al.* (CDF Collaboration), Phys. Rev. D **82**, 052002 (2010); T. Aaltonen *et al.* (CDF Collaboration), Phys. Rev. D **81**, 052011 (2010).

[9] A. Abulencia *et al.* (CDF Collaboration), Phys. Rev. Lett. **96**, 202002 (2006).

[10] D. Acosta *et al.* (CDF Collaboration), Phys. Rev. D **71**, 052003 (2005).

[11] D. Acosta *et al.* (CDF Collaboration), Phys. Rev. D **71**, 032001 (2005).

[12] A. Abulencia *et al.* (CDF Collaboration), Phys. Rev. Lett. **97**, 082004 (2006).

[13] A. Abulencia *et al.* (CDF Collaboration), J. Phys. G Nucl. Part. Phys. **34** (2007).

[14] R. Blair *et al.* (CDF Collaboration), FERMILAB-Pub-96/390-E (1996).

[15] F. Abe *et al.* (CDF Collaboration), Phys. Rev. D **45**, 1448 (1992).

[16] A. Bhatti *et al.*, Nucl. Instrum. Meth. A **566** 375 (2006).

[17] T. Aaltonen *et al.* (CDF Collaboration). Phys. Rev. Lett. **105**, 012001 (2010).

[18] T. Sjostrand *et al.*, Comput. Phys. Commun. **135** 238 (2001).

[19] E. Gerchtein and M. Paulini, CHEP-2003-TUMT005, arXiv:physics/0306031 (2003).

[20] Tevatron Electroweak Working Group (CDF, D0 Collaborations), arXiv:1007.3178v1 [hep-ex] (2010).

[21] V. D. Barger and R. J. N. Phillips, **Collider Physics**, *Addison-Wesley* (1987).

[22] R. Brun and F. Rademaker, ROOT Version 4.00/08, http://root.cern.ch/, class TMultiLayerPerceptron.

[23] G. Corcella *et al.*, JHEP **01**, 10 (2001).

[24] H. L. Lai *et al.*, Eur. Phys. J. C **12**, 375 (2000).

[25] A. D. Martin, R. G. Roberts, W. J. Stirling and R. S. Thorne, Eur. Phys. J. C **4**, 463 (1998).

[26] P. Skands, D. Wicke, Nuovo Cim. B **123** S1 (2008).

[27] V. Ahrens *et al*, J. High Energy Phys. **09**, 097 (2010); N. Kidonakis, arXiv:1009.4935 [hep-ph] (2010); M. Cacciari *et al*, J. High Energy Phys. **0809**, 127 (2008).